J. Micropalaeontology, 44, 497–507, 2025
https://doi.org/10.5194/jm-44-497-2025

Journal of Micropalaeontology
Open Access

Pliocene to modern Southern Ocean diatom biostratigraphy revised using samples from IODP Expedition 382

Jonathan P. Warnock[1], Brendan T. Reilly[2], Linda Armbrecht[3], and Yuji Kato[4]

[1]Anthropology, Geospatial and Earth Sciences, Indiana University of Pennsylvania, Indiana, PA 15701, USA
[2]Biology and Paleo Environment, Lamont-Doherty Earth Observatory, Palasades, NY, 10964, USA
[3]Institute for Marine and Antarctic Studies, University of Tasmania, Hobart, TAS, Australia
[4]Marine Core Research Institute, Kochi University, Monobe, Nankoku, Kochi 783-8502, Japan

Correspondence: Jonathan P. Warnock (jwarnock@iup.edu)

Received: 3 June 2024 – Revised: 25 March 2025 – Accepted: 6 April 2025 – Published: 10 November 2025

Abstract. Biostratigraphy is frequently used to generate age models and is significant to understanding the rate and timing of Cenozoic climate change. Records from the Southern Ocean (SO) are particularly valuable in understanding the past behavior of the Antarctic Ice Sheet, whereby clues to this behavior can be gained from the presence and composition of preserved microfossils. Diatoms, a nearly ubiquitous group of microalgae that make cell walls out of opal, preserve well in Southern Ocean sediments and have been used extensively in Southern Ocean biostratigraphy. Here, we present an updated diatom biostratigraphy of the Southern Ocean extending 3.3 Myr from sediments recovered during International Ocean Discovery Program (IODP) Expedition 382 "Iceberg Alley" Site U1537. Furthermore, we compare a tuned age model to a paleomagnetic-based age model to provide two independent estimates of ages of these datums with quantified uncertainty. The high sedimentation rate found at Site U1537 allows detailed age assessment, allowing the generation of more finely tuned age models in Southern Ocean sediments.

1 Introduction

Biostratigraphy is used extensively as a technique to assign ages to sediments and sedimentary rocks. In Quaternary and Neogene sediments, ages are often assigned via correlation to benthic $\delta^{18}O$ (commonly, the LR04 stack; Lisiecki and Raymo, 2005) or Antarctic ice cores (e.g., Weber et al., 2022). Accurately assigning ages to sedimentary records of past climate change is vital to understanding the rate of ice sheet mass loss over the coming decades and centuries. Records from the Southern Ocean (SO) are particularly useful in understanding the behavior of the Antarctic Ice Sheet (e.g., Konfirst et al., 2012; Bailey et al., 2022; Warnock et al., 2022). Carbonate microfossils are often used in biostratigraphic and orbitally tuned age models; however, they rarely preserve in Southern Ocean sediments. Diatoms, single-celled marine algae found in nearly all habitats on Earth with light and water, which make their cell walls out of hydrated amorphous silica (opal, $SiO_2 \cdot nH_2O$), preserve well in Southern Ocean sediments (Warnock and Scherer, 2015).

Diatoms have been used extensively as Southern Ocean biostratigraphic markers. Early work began with the Deep Sea Drilling Project (DSDP), establishing significant biostratigraphic markers and zones (e.g., McCollum, 1975; Gombos, 1983). Refinements of biostratigraphic markers in both the Paleogene (Barron, 2003) and the Neogene (e.g., Gersonde and Burckle, 1990; Winter and Iwai, 2002; Kato et al., 2016) were made possible with additional Southern Ocean drilling under the Ocean Drilling Project (ODP). Southern Ocean drilling and related diatom-based biostratigraphic zonations were published under the Integrated Ocean Drilling Program/International Ocean Discovery Program (IODP; e.g., Whitehead and Bohaty, 2003). In addition to these deep-water sites, drilling on the continent allowed further refinement of biostratigraphy during the Cape Roberts

Project (CRP; e.g., Harwood and Bohaty, 2001; Olney et al., 2007) and the Antarctic Drilling Project (ANDRILL; e.g., Winter et al., 2012; Sjunneskog and Winter, 2012). While these studies have provided useful biostratigraphic information for understanding Cenozoic climate change, they are constrained by recovery breaks of the drilled sediments and low sedimentation rates that provide limited detail on the associated time zones captured. A significant advance in SO diatom biostratigraphy came from the utilization of constrained optimization to produce an idealized biostratigraphy from all available Southern Ocean data, rather than one site at a time (Cody et al., 2008, 2012). While these studies provided a valuable new framework for utilizing SO diatoms, they are based on previous biostratigraphic studies and are therefore also associated with low recovery and low sedimentation rate intervals. Here, we present an updated Southern Ocean diatom biostratigraphy spanning the last 3.3 Myr from a Scotia Sea contourite deposit. We compare an age model based on climate correlation to the EPICA Dome C (EDC) (0–800 ka) and LR04 stack (800–1500 ka) (Weber et al., 2022) to a paleomagnetic age model (0–3300 ka) (Reilly et al., 2021) and discuss the uncertainties associated with each approach. This study offers new perspective in providing a biostratigraphy from a deep-sea area with high sedimentation rates and fairly continuous accumulation (Weber et al., 2021). The sedimentation rate is 6.1 cm kyr^{-1} in the lower portions of the core and increases to 14.8 cm kyr^{-1} upcore where opal accumulation is higher.

Site information

The sediments used for this analysis were recovered as part of IODP Expedition 382, "Iceberg Alley and Subantarctic Ice and Ocean Dynamics", which drilled the Dove (sites U1536 and U1537) and Pirie (Site U1538) basins of the Scotia Sea (Fig. 1). Site U1537 is located at 59°6.65′ S, 40°54.37′ W with a water depth of 3713 m (Weber et al., 2021). Icebergs calved from around Antarctica are directed towards the Dove Basin, giving this area the name "Iceberg Alley" (Anderson and Andrews, 1999). These icebergs release terrigenous sediment and nutrients when they melt via interaction with the relatively warmer water of the Antarctic Circumpolar Current (ACC; Budge and Long, 2018). Site U1537 was drilled on a contourite deposit affected by Antarctic Bottom Water (Pérez et al., 2021). The recovered sediments are comprised of diatom ooze and diatom-bearing silty clay (Weber et al., 2021). High sedimentation rates up to 100 cm kyr^{-1} make this area ideal for recovering high-resolution records of Antarctic and Southern Ocean change (Weber et al., 2021) and provide the opportunity to refine biostratigraphic datums. Samples were taken from holes A and D of Site U1537.

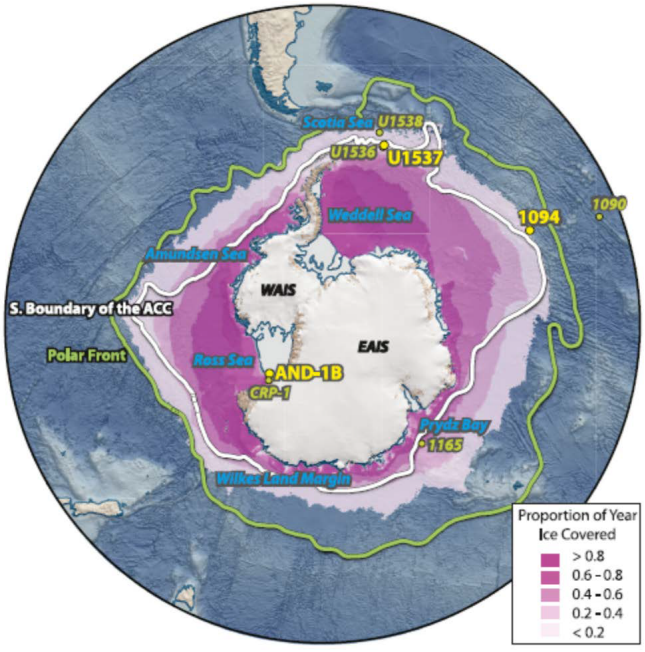

Figure 1. Map. This figure shows the site location and the locations of a selection of other significant sites. Purple shading indicates the proportion sea-ice coverage during the year, based on data from 2002 to 2011 (Spreen et al., 2005). Colored lines indicate the position of the southern boundary of the Antarctic Circumpolar Current (white) and the Polar Front (green) (Orsi et al., 1995). Map created with Quantarctica (Matsuoka et al., 2021) using ETOPO1, IBSCO, and RAMP2 data (Amante and Eakins, 2009; Arndt et al., 2013; Liu et al., 2016). AP: Antarctic Peninsula; WAIS: West Antarctic Ice Sheet; EAIS: East Antarctic Ice Sheet; EDC: EPICA Dome C.

2 Methods

Samples utilized for this study were collected aboard the D/V *JOIDES Resolution* during Expedition 382. For preliminary shipboard diatom biostratigraphic analysis, each core catcher was sampled with a toothpick and prepared by smearing sediment in a small quantity of water across the slide (i.e., a "smear slide"). Slides were set with Norland Optical Adhesive No. 61. In addition to shipboard sampling, U1537 paleomagnetic cube samples were also toothpick-sampled to refine the resolution of the diatom datums, providing material at a resolution of about 1 per section, or ∼ 1.5 m. However, higher-resolution sampling was used to narrow down datum positions when possible. Samples were taken from Hole A for cores 1 to 31 and from Hole D for cores 34 to 50. Smear slides were used for these samples as well. A total of 124 microslides were made. All slide depths can be found in Table S1 in the Supplement. Diatom species identifications follow those of Weber et al. (2021) and Warnock et al. (2022). Three full transects (44 mm each) were counted on each slide, yielding between 100 and 300 valves. Much like biostratigraphic markers, taxonomic concepts for SO di-

atoms were developed from scientific drilling on the continental shelf and deeper water by DSDP, ODP, and IODP (McCollum, 1975; Schrader, 1976; Gombos, 1976; Ciesielski, 1983; Gersonde and Burckle, 1990; Gersonde, 1991; Gersonde et al., 1990; Fenner, 1991; Baldauf and Barron, 1991; Harwood and Maruyama, 1992; Mahood and Barron, 1996; Gersonde and Bárcena, 1998; Censarek and Gersonde, 2002; Iwai and Winter, 2002; Zielinski and Gersonde, 2002; Arney et al., 2003; Bohaty et al., 2003; Whitehead and Bohaty, 2003). Efforts closer to the continent have provided additional taxonomic clarity, especially for shallow-water- and sea-ice-related species (Harwood, 1986, 1989; Winter and Harwood, 1997; Bohaty et al., 1998; Harwood et al., 1998; Scherer et al., 2000; Sjunneskog and Scherer, 2005; Olney et al., 2007, 2009; Sjunneskog et al., 2012; Winter et al., 2012). All species identifications and data collections were conducted at 1000× magnification, and data were primarily collected on a presence/absence basis.

Age model

The orbitally tuned age model of Weber et al. (2022) was used to evaluate the timing of biostratigraphic events from 0 to 1.5 Ma, the furthest it has been extended. This age model was generated via correlation of the U1537 magnetic susceptibility record to the EPICA Dome C (EDC) dust record for the last 0.8 Myr and to the LR04 benthic δ^{18}O record for 0.8–1.5 Ma (Weber et al., 2022; hereafter W22), with uncertainty in tie points propagated using the Undatable age–depth modeling tool (Lougheed and Obrochta, 2019). The age model was tuned to the LR04 benthic stack in order to provide as detailed an age model as possible, due to the clear correlations between the benthic stack and physical properties of the core from Site U1537 (Lisiecki and Raymo, 2005; Weber et al., 2022). The paleomagnetic age model of Reilly et al. (2021; hereafter R21) and its uncertainty estimates were used to assess biostratigraphic datums from 0 to 3.3 Ma. From 0–1.5 Ma, the R21 age model requires fewer assumptions than W22 about how U1537 climate signals relate to regional and global climate, but it also has significantly larger uncertainty. Both age models are in agreement around the magnetic reversals, and the W22 age model falls within the R22 uncertainty structure (Fig. 2). The R21 age model is extended linearly to 3.549 Ma in order to include key diatom taxa using the Gauss–Gilbert Chron boundary, as identified by Reilly et al. (2021); however, the U1537 stratigraphy between ∼3.3 and 3.6 Ma becomes more complex, and accumulation rates are likely variable (Reilly et al., 2021; Weber et al, 2021).

3 Results

The age models of Weber et al. (2022) and Reilly et al. (2021) differ more with increasing distance from each paleomagnetic reversal, as Weber et al. (2022) allows a variable sedimentation rate, whereas the median age of the Reilly et al. (2021) uncertainty structure is similar to assuming linear sedimentation rates between reversals (Fig. 2). A linear sedimentation rate lasting for 773 kyr, i.e., the length of the Brunhes Chron (Gradstein et al., 2020), is highly unlikely due to glacial–interglacial variations in sediment focusing and supply in the Scotia Sea (Sprenk et al., 2013) and due to a long-term increase in accumulation rates at Site U1537 since 3.3 Ma (Weber et al., 2022; Reilly et al., 2021). The age model of Weber et al. (2022) shows a strong correlation with the well-dated EPICA Dome C (EDC) ice core dust record over the last 0.8 Myr (Lambert et al., 2008; Weber et al., 2022), allowing confidence in its assigned ages over that interval. Only the age model of Reilly et al. (2021) is available prior to 1.5 Ma; therefore biostratigraphic events are only dated using the age model of Reilly et al. (2021) for the interval from 1.5 to 3.6 Ma (to 340.1 m composite depth (mcd)). Paleomagnetic reversals are more common during this interval than from 0–0.8 Ma, resulting in lower uncertainty. Table 1 gives the timing of biostratigraphic events as determined by this analysis. Figure 3 provides a range chart for the analyzed species. Zonal definitions follow modern schemes, the most recent in the Southern Ocean being Winter et al. (2012), which was developed from the scheme of Winter and Iwai (2002). Some biozone names from older works, e.g., Zielinski and Gersonde (2002), were not used in Winter et al. (2012) and so are not used here. Furthermore, both Winter and Iwai (2002) and Winter et al. (2012) utilized samples taken closer to the continent than those of Zielinski and Gersonde (2002). Given that Site U1537 is much nearer the continent than the sites utilized by Gersonde and Zielinski, Winter et al. (2012) is used here. Zonal definitions and ages are as follows.

Zonal definitions

Thalassiosira lentiginosa partial range zone

Author: McCollum (1975), renamed by Kellogg and Kellogg (1986), updated by Zielinski and Gersonde (2002) modified by Winter et al. (2012)

Definition of top: last occurrence (LO) of *Thalassiosira lentiginosa* (extant)

Definition of base: LO of *Actinocyclus ingens*

Age: 0–0.527 Ma

Biostratigraphic events contained within this zone: LO of *R. leventerae* at 0.121 Ma; LO of *Hemidiscus karstenii* at 0.252 Ma; LO of *Rouxia constricta* at 0.426 Ma.

Actinocyclus ingens partial range zone

Author: Gersonde and Burckle (1990), updated by Winter et al., 2012, who defined base of this zone as the LO *R.*

Table 1. This table provides age/depth comparisons for selected diatom species from site U1537. Abbreviations follow those used in the text. Age errors were calculated following the methods of Lougheed and Obrochta (2019), Reilly et al. (2021), and Weber et al. (2022). mcd: meters composite depth.

Event	Species	Samples (top/bottom)	Event depth (mcd)	Calculated age (Ma)
LO	*R. leventerae*	4H-3, 75–76 cm/4H-4, 75–76 cm	26.005 ± 0.75	0.121 ± 0.003
LO	*H. karstenii*	6H-7 25–27 cm/6H CC	49.99 ± 0.24	0.252 ± 0.002
LO	*R. constricta*	8H CC/9H CC	74.06 ± 4.87	0.426 ± 0.004
LO	*A. ingens*	9H CC/10H CC	83.58 ± 4.60	0.527 ± 0.002
LO	*Rh. harwoodii*	10H CC/11H-1, 50–51 cm	88.36 ± 0.14	0.534 ± 0.002
FO	*Th. antarctica*	11H-2, 50–51 cm/11H-2, 126–128 cm	91.14 ± 0.036	0.551 ± 0.002
LO	*Th. elliptipora*	11H-5, 60–62 cm/11H-3, 50–51 cm	94.23 ± 0.38	0.588 ± 0.002
FO	*P. glacialis*	11H-6, 70–72 cm/11H-7, 31–33 cm	96.79 ± 0.55	0.602 ± 0.002
LO	*Th. fasciculata*	14H-3, 50–51 cm/14H-2 50–51 cm	118.51 ± 1.50	0.928 ± 0.004
FO	*R. constricta*	15H-CC/16H-CC	140.62 ± 4.76	1.074 ± 0.003
FO	*F. separanda*	17H-CC/18H-1, 120–122 cm	155.39 ± 0.31	1.242 ± 0.005
LO	*Th. kolbei*	17H CC/18H-1, 120–121 cm	155.39 ± 0.31	1.261 ± 0.004
LO	*F. barronii*	19H CC/20H-1, 50–51 cm	173.66 ± 0.34	1.438 ± 0.004
LO	*F. robusta*	19H CC/20H-1, 50–51 cm	173.66 ± 0.34	1.438 ± 0.004
LO	*S. tetraoestrupii* var. *reimeri*	20H-2, 50–51 cm/20H-3, 50–51 cm	176.26 ± 0.75	1.465 ± 0.004
FO	*F. obliquecostata*	22H-1, 50–51 cm/22H-1, 130–132 cm	193.41 ± 0.40	1.630 ± 0.049
FO	*F. kerguelensis*	25H-3, 16–18 cm/25H-4, 40–42 cm	225.24 ± 1.06	2.127 ± 0.003
LO	*R. antarctica*	22H-1, 50–51 cm/22H-1, 130–132 cm	193.41 ± 0.40	1.637 ± 0.025
LO	*A. karstenii*	22H-1, 130–132 cm/22H-2, 100–102 cm	194.41 ± 0.59	1.648 ± 0.043
LO	*F. bohatyi*	22H-3, 70–72/22H-4, 40–42 cm	196.81 ± 0.59	1.670 ± 0.031
LO	*Th. inura*	22H-4, 40–42 cm/22H-5, 100–102 cm	196.81 ± 0.59	1.670 ± 0.031
LO	*Th. torokina*	22H-4, 40–42 cm/22H-5, 100–102 cm	196.81 ± 0.59	1.670 ± 0.031
LO	*A. fasciculatus*	22H-4, 40–42 cm/22H-5, 100–102 cm	196.81 ± 0.59	1.670 ± 0.031
LO	*R. diploneides*	24H CC/25H-1, 125–127 cm	221.54 ± 0.72	2.079 ± 0.012
LO	*R. naviculoides*	24H CC/25H-1, 125–127 cm	221.54 ± 0.72	2.079 ± 0.012
LO	*Th. vulnifica*	25H-1, 125–127 cm/25H-2, 14–16 cm	222.46 ± 0.19	2.089 ± 0.009
FO	*S. gracilis*	25H-CC/26H-1, 98–100 cm	230.93 ± 0.56	2.211 ± 0.002
FO	*Th. ritscheri*	25H-CC/26H-1, 98–100 cm	230.93 ± 0.56	2.211 ± 0.002
FO	*Th. scotia*	25H-CC/26H-1, 98–100 cm	230.93 ± 0.56	2.211 ± 0.002
LO	*Th. insigna*	26H-1, 98–100 cm/26H-2, 80–82 cm	231.95 ± 0.44	2.244 ± 0.027
LO	*F. interfrigidaria*	27H-2, 80–82 cm/27H-3, 85–87 cm	243.09 ± 0.77	2.404 ± 0.059
FO	*A. fasciculatus*	28F-2, 75–77 cm/28F-3, 50–52 cm	247.69 ± 0.62	2.454 ± 0.047
FO	*R. leventerae*	28F-4, 30–32 cm/28F-CC	249.46 ± 0.17	2.483 ± 0.038
LO	*F. weaveri*	28F-4, 30–32 cm/28H CC	249.46 ± 0.17	2.487 ± 0.038
LO	*Th. complicata*	30F-3, 56–58 cm/30F-CC	258.63 ± 0.66	2.657 ± 0.015
FO	*F. curta*	31F-1, 60–62 cm/31F-2, 57–59 cm	260.55 ± 0.73	2.687 ± 0.022
FO	*A. maccollumii*	U1537A 31F-CC/U1537D 34F-4, 53–55 cm	270.77 ± 6.50	2.791 ± 0.047
FO	*F. weaveri*	34F-CC/35F-1, 60–62 cm	277.91 ± 0.20	3.187 ± 0.008
LO	*F. praeinterfrigidaria*	36F-CC/37F-1, 75 cm	287.23 ± 0.63	3.354 ± 0.009
LO	*P. barboi*	37F-3, 74–75 cm/38F-CC	293.50 ± 2.64	3.412 ± 0.023
LO	*R. heteropolara*	40F-CC/41F-1, 75–76 cm	306.77 ± 0.28	3.491 ± 0.031
FO	*Th. elliptipora*	41F-1, 75–76 cm/42F-2, 75–76 cm	307.78 ± 0.72	3.491 ± 0,031
FO	*A. ingens*	41F-3, 75–76 cm/41F-4, 75–76 cm	310.52 ± 0.54	3.501 ± 0.028
LO	*F. fossilis*	41F-2, 75–76 cm/41F-3, 75–76 cm	307.78 ± 0.72	3.501 ± 0.028
FO	*F. ritscheri*	41F-2, 75–76 cm/41F-3, 75–76 cm	309.24 ± 0.74	3.501 ± 0.028
FO	*F. robusta*	41F-2, 75–76 cm/41F-3, 75–76 cm	309.24 ± 0.74	3.501 ± 0.028
FO	*H. karstenii*	41F-2, 75–76 cm/41F-3, 75–76 cm	309.24 ± 0.74	3.501 ± 0.028
FO	*Rh. harwoodii*	41F-2, 75–76 cm/41F-3, 75–76 cm	309.24 ± 0.74	3.501 ± 0.028
LO	*Th. striata*	41F-1, 75–76 cm/42F-2, 75–76 cm	307.78 ± 0.72	3.501 ± 0.028
FO	*Th. torokina*	41F-2, 75–76 cm/41F-3, 75–76 cm	309.24 ± 0.74	3.501 ± 0.028
FO	*Th. tumida*	41F-2, 75–76 cm/41F-3, 75–76 cm	309.24 ± 0.74	3.501 ± 0.028
FO	*P. barboi*	41F-4, 75–76 cm/42F-CC	313.24 ± 2.16	3.518 ± 0.023
FO	*Th. fasciculata*	41F-4, 75–76 cm/42F-CC	313.24 ± 2.16	3.518 ± 0.023
FO	*Th. lentiginosa*	41F-4, 75–76 cm/42F-CC	313.24 ± 2.16	3.518 ± 0.023
FO	*Th. oliverana*	41F-4, 75–76 cm/42F-CC	313.24 ± 2.16	3.518 ± 0.023

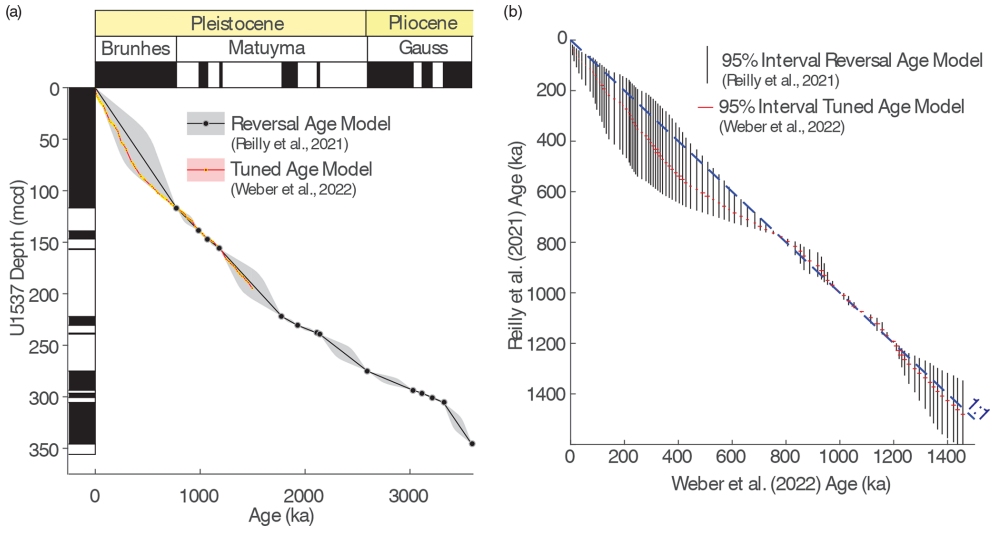

Figure 2. Age–depth model comparison. This figure compares the age–depth models between the paleomagnetically based results of Reilly et al. (2021) versus the orbitally tuned results of Weber et al. (2022). The Weber model is preferred for the most recent 1400 kyr due to increased accuracy and number of tie points. In panel **(a)**, black dots represent reversal tie points in Reilly et al. (2021), and the gray shading represents the error. The yellow dots represent tie points in the Weber et al. (2022) model, and associated red bars are the errors in that model. In panel **(b)**, the errors in age models are compared between Reilly et al. (2021; black columns) and Weber et al. (2022; red bars). mcd: meters composite depth.

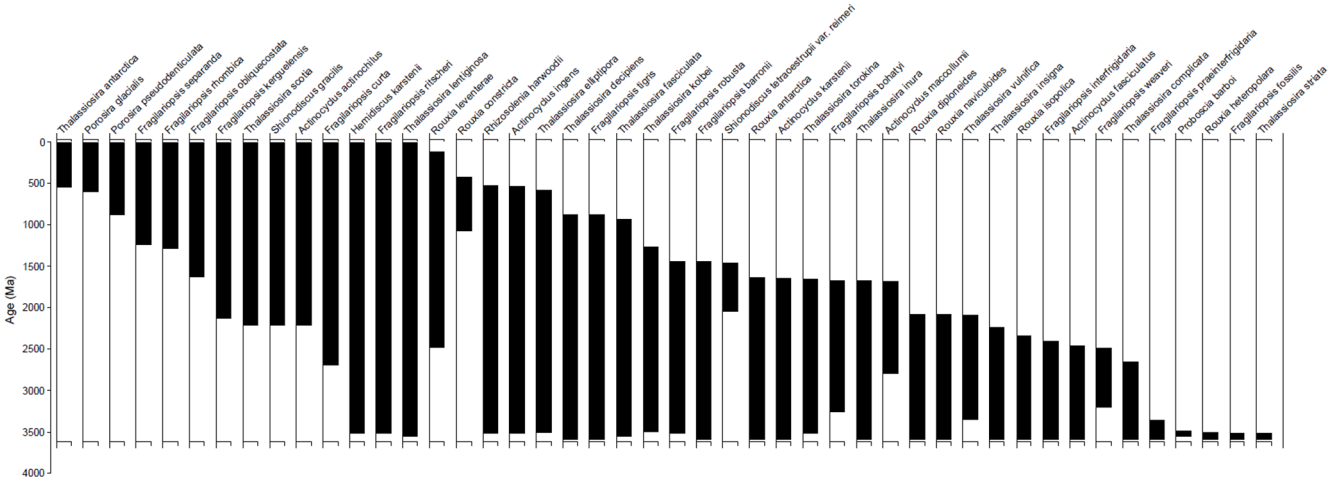

Figure 3. Biostratigraphic range model. This figure shows the age range for the diatoms utilized in this study.

antarctica. Here, we redefine the base back to the LO of *Thalassiosira kolbei* due to the order of observed biostratigraphic events at Site U1537.

Definition of top: LO *A. ingens*

Definition of base: LO *Th. kolbei*

Age: 0.527–1.261 Ma

Biostratigraphic events contained within this zone: LO of *Rhizosolenia harwoodii* at 0.534 Ma; first occurrence (FO) of *Th. antarctica* at 0.551 Ma; LO of *Th. elliptipora* at 0.588 Ma; FO of *Porosira glacialis* at 0.602 Ma; LO of *Th. fasciculata* at 0.928 Ma; FO of *R. constricta* at 1.074 Ma; FO of *Fragilariopsis separanda* at 1.242 Ma.

Thalassiosira kolbei partial range zone

Author: Ciesielski (1983), renamed by Baldauf and Barron (1991), replaced with *Rouxia antarctica* partial range zone by Winter et al. (2012)

Definition of top: LO *Th. kolbei*

Definition of base: LO *Rouxia antarctica*

Age: 1.261–1.637 Ma

Biostratigraphic events contained within this zone: LO of *F. barronii* at 1.438 Ma; LO of *F. robusta* at 1.438 Ma; LO of *Shionodiscus tetraoestrupii* var. *reimeri* at 1.465 Ma; FO of *F. obliquecostata* at 1.630 Ma.

Rouxia antarctica partial range zone

Author: Sjunneskog and Winter (2012)

Definition of top: LO *R. antarctica*

Definition of base: LO *A. fasciculatus*

Age: 1.637–1.670 Ma

Biostratigraphic events contained within this zone: LO of *Actinocyclus karstenii* at 1.648 Ma; LO of *F. bohatyi* at 1.670 Ma; LO of *Th. inura* at 1.670 Ma; LO of *Th. torokina* at 1.670 Ma.

Actinocyclus fasciculatus/Act. maccollumii Concurrent range zone

Author: Winter et al. (2012)

Definition of top: LO *A. fasciculatus*

Definition of base: FO *A. maccollumii*

Age: 1.670–2.791 Ma

Biostratigraphic events contained within this zone: LO of *R. diploneides* at 2.079 Ma; LO of *R. naviculoides* at 2.079 Ma; LO of *Th. vulnifica* at 2.098 Ma; FO of *Shionodiscus gracilis* at 2.211 Ma; FO of *Th. ritscheri* at 2.211 Ma; FO of *Th. scotia* at 2.211 Ma; FO of *F. kerguelensis* at 2.127 Ma; LO of *Th. insigna* at 2.244 Ma; LO of *F. interfrigidaria* at 2.404 Ma; FO of *A. fasciculatus* at 2.454 Ma; FO of *R. leventerae* at 2.483 Ma; LO of *F. weaveri* at 2.487 Ma; LO of *Th. complicata* at 2.657 Ma; FO of *F. curta* at 2.687 Ma.

Fragilariopsis interfrigidaria partial range zone

Author: McCollum, 1975, updated by Weaver and Gombos (1981), Harwood and Maruyama (1992), and Winter et al. (2012)

Definition of top: FO *A. maccollumii*

Definition of bottom: FO *F. interfrigidaria*

Age 2.791–3.549 Ma

Biostratigraphic events contained within this zone: FO of *F. weaveri* at 3.187; LO of *F. praeinterfrigidaria* at 3.354 Ma; LO of *P. barboi* at 3.412 Ma; LO of *R. heteropolara* at 3.491 Ma; FO of *Th. elliptipora* at 3.491 Ma; FO of *A. ingens* at 3.501 Ma; LO of *F. fossilis* at 3.501 Ma; FO of *F. ritscheri* at 3.501 Ma; FO of *F. robusta* at 3.501 Ma; FO of *H. karstenii* at 3.501 Ma; FO of *Rh. harwoodii* at 3.501 Ma; LO of *Th. striata* at 3.501 Ma; FO of *Th. torokina* at 3.501 Ma; FO of *Th. tumida* at 3.501 Ma; FO of *P. barboi* at 3.518 Ma; FO of *Th. fasciculata* at 3.518 Ma; FO of *Th. lentiginosa* at 3.518 Ma; FO of *Th. oliverana* at 3.518 Ma.

4 Discussion and conclusions

The high sedimentation rate of Site U1537 and continuous sedimentation allowed detailed refinement of Southern Ocean diatom biostratigraphic markers. The difference between this and other Southern Ocean diatom-based biostratigraphic models varies with age and geography. Gersonde and Bárcena (1998) updated Southern Ocean diatom biostratigraphy utilizing existing sediments and novel gravity core material. Differences between that age model and the one presented here are variable. Gersonde and Bárcena (1998) place the LO of *A. ingens* at 0.65 Ma, whereas we place it at 0.527 Ma. Often, the ages presented by Gersonde and Bárcena (1998) are ranges, whereas the ages presented here are specific. For example, they place the LO of *Th. kolbei* at 2.0–1.8 Ma, whereas we place it at 1.261 Ma. Other differences are smaller, e.g., the LO of *Th. vulnifica* at 2.6–2.5 Ma (Gersonde and Bárcena, 1998) compared to 2.550 Ma in this study.

Zielinski and Gersonde (2002) analyzed sediments from ODP Leg 177 in the Atlantic sector of the Southern Ocean. Ages tend to vary by 0.1 Myr or less. For example, we find the LO of *H. karstenii* to have occurred at 0.252 Ma, whereas Zielinski and Gersonde (2002) place it at 0.184 Ma utilizing sediment from ODP sites 1089 through 1094. We place the LO of *Th. fasciculata* at 0.928 Ma compared to 0.87 Ma (Zielinski and Gersonde, 2002).

More recently still, Kato et al. (2024) published a diatom- and radiolarian-based biostratigraphy from the Atlantic sector of the Southern Ocean using materials from ODP Site 697. This paper provided ages for biostratigraphic events for the early and middle Pliocene. Their datums are generally within 0.2 Ma of ours, for example, the LO of *F. praeinterfrigidaria* at 3.18 Ma (Kato et al., 2024) compared to 3.354 Ma (this study). The LO of *Th. lentiginosa* is placed at 3.47 Ma by Kato et al. (2024) and at 3.518 Ma here. A large difference was found in the LO of *Th. complicata*, however. Kato et al. (2024) place the datum at 3.11 Ma, whereas this paper finds it at 2.657 Ma. Given the large discrepancy and the possibility of reworking in Iceberg Alley, the date provided by Kato et al. (2024) is likely more valid.

When considering biostratigraphic schemes from the Ross Sea, the older the datum, the larger the difference between these data and previously published zonations (e.g., Winter et al., 2012). For example, Winter et al. (2012) place the LO of *Actinocyclus ingens* at 0.54 Ma, whereas we place it at 0.527 Ma. These small shifts in the timing of biostratigraphic events could represent local ecological factors, e.g., diachronous timing of ecological temperature and nutrient thresholds around the continent. Alternatively, these shifts could simply represent the refinement of the timescale afforded by the unusually high sedimentation rate at Site U1537. Given the error in dating techniques used to assign ages to diatom biostratigraphic markers and the relative scarcity of SO sediment cores, it is impossible to dis-

Table 2. This table compares biostratigraphic datum ages from this study to those of Cody et al. (2008) and Crampton et al. (2016).

Event	Species	Average range model (Cody et al., 2008)	Published age as reported in Cody et al. (2008)	Composite mid-age as reported in Crampton et al. (2016)	Calculated age (this study)
LO	*R. leventerae*	0.07–0.35	0.13–0.14	N/A	0.121
LO	*H. karstenii*	0.28–0.33	0.35–0.43	0.16	0.252
LO	*R. constricta*	0.43–0.05	0.28–0.3	N/A	0.426
LO	*A. ingens*	0.5–0.57	0.3–1.99	0.08	0.527
LO	*Rh. harwoodii*	N/A	N/A	0.39	0.534
FO	*Th. antarctica*	0.57–0.64	N/A	0.23	0.551
LO	*Th. elliptipora*	0.64–0.71	0.3–1.81	0.85	0.588
FO	*P. glacialis*	1.07–1.23	N/A	N/A	0.602
LO	*Th. fasciculata*	0.89	0.75–1.81	0.70	0.928
FO	*R. constricta*	1.04–1.23	0.91–1.61	N/A	1.074
FO	*F. separanda*	1.37–1.45	N/A	0.47	1.242
LO	*Th. kolbei*	1.98–1.98	1.61–2.7	1.98	1.261
LO	*F. barronii*	1.19–1.29	0.8–2.6	1.54	1.438
LO	*F. robusta*	N/A	N/A		1.438
LO	*S. tetraoestruppii* var. *reimeri*	1.31–1.34	1.32–1.61	1.86	1.465
FO	*F. obliquecostata*	1.66–1.73	N/A	N/A	1.63
LO	*R. antarctica*	1.48–1.51	1.35–1.57	1.31	1.637
LO	*A. karstenii*	2.13–2.16	1.81–2.91	0.92	1.648
LO	*F. bohatyi*	N/A	N/A	N/A	1.67
LO	*Th. inura*	2.53–2.55	1.88–3.1	2.26	1.67
LO	*Th. torokina*	2.2–2.27	1.88–2.18	0.62	1.67
LO	*A. fasciculatus*	2.05–2.27	1.81–2.81	2.02	1.67
LO	*R. diploneides*	2.55–2.69	2.51	2.42	2.079
LO	*R. naviculoides*	2.28–2.32	N/A	2.34	2.079
LO	*Th. vulnifica*	2.15–2.19	0.6–3.1	2.06	2.098
FO	*F. kerguelensis*	2.18–2.21	1.2–3.23	2.22	2.127
FO	*S. gracilis*	1.87	2.29	0.55	2.211
FO	*Th. ritscheri*	N/A	N/A	N/A	2.211
FO	*Th. scotia*	N/A	N/A	N/A	2.211
LO	*Th. insigna*	2.45–2.5	1.81–4.61	2.38	2.244
LO	*F. interfrigidaria*	2.4–2.45	1.81–3.3	2.75	2.404
FO	*R. leventerae*	2–2.08	N/A	N/A	2.483
FO	*A. fasciculatus*	2.05–2.27	1.81–2.81	2.62	2.454
LO	*F. weaveri*	2.45–2.53	1.81–3.71	2.18	2.487
LO	*Th. complicata*	3.36–3.44	2.61–4.51	2.70	2.657
FO	*F. curta*	3.54–3.57	3.72	4.56	2.687
FO	*A. maccollumii*	2.79–2.84	2.5–3.3	2.83	2.791
FO	*F. weaveri*	3.51–3.55	3.1–4.31	3.44	3.187
LO	*F. praeinterfrigidaria*	3.45–3.49	2.09–4.61	2.99	3.354
LO	*P. barboi*	1.61–1.73	1.61–4.2	2.87	3.412
LO	*R. heteropolara*	3.42–3.47	2.2–2.61	3.74	3.491
FO	*Th. elliptipora*	2–2.06	1.07–3.51	3.50	3.491
FO	*A. ingens*	15.84–15.89	14.78–17.43	15.6	3.501
LO	*F. fossilis*	∼ 2.86–2.92	0.7–0.99	3.54	3.501
FO	*F. ritscheri*	2.82–2.88	3.6	3.56	3.501
FO	*F. robusta*	N/A	N/A	N/A	3.501
FO	*H. karstenii*	9.68–10.24	9.64	10.2	3.501
FO	*Rh. harwoodii*	N/A	N/A	4.52	3.501
LO	*Th. striata*	2.89–2.96	1.81–3.51	4.61	3.501
FO	*Th. torokina*	6.43–8.03	8.56–10.07	9.36	3.501
FO	*Th. tumida*	4.23–4.37	N/A	4.82	3.501
FO	*P. barboi*	∼ 13–13.3	11.47–12.77	19.18	3.518
FO	*Th. fasciculata*	4.25–4.42	4.49	4.58	3.518
FO	*Th. lentiginosa*	3.86–4.11	2.89–4.91	4.04	3.518
FO	*Th. oliverana*	∼ 5.14–7.21	6.61	9.74	3.518

N/A – not available.

tinguish between these factors. However, a single circum-Antarctic diatom biostratigraphy, rather than regional biostratigraphies, is generally used to assign ages to sediment (Sjunneskog and Winter, 2012); thus, we argue for the use of most of the dates generated here due to the high sedimentation rate. While the Northern and Southern ACC have previously been divided biostratigraphically (Zielinski and Gersonde, 2002), other biostratigraphic schemes ignore this dichotomy (e.g., Winter et al., 2012) The scheme of Cody et al. (2012) based on constrained optimization (CONOP) does not utilize this dichotomy. Some discrepancies are larger; for example, the LOD of *A. ingens* is found at ∼ 0.38 Ma by Zielinski and Gersonde (2002) and Tolotti et al. (2018). Sampling resolution is similar between the studies, with sampling every 1.5 m. Discrepancies may reflect local ecological factors; however, sampling and sample counting are unlikely to have caused these differences.

It has been noted that SO diatom biostratigraphic dates are often based on poor-quality paleomagnetic records (Tauxe et al., 2012). When detailed paleomagnetic timescales are available, biostratigraphic datums can be well refined (Tauxe et al., 2012). The high sedimentation rate, the detailed and tuned age model over the upper 1.5 Myr (Weber et al., 2022), and the detailed high-quality magnetostratigraphic age model from 1.5 to 3.3 Ma make the ages presented here a significant improvement on previously established datums.

A circum-Antarctic diatom biostratigraphy, generated by using constrained optimization (CONOP) statistical techniques, has been developed and updated in recent years (Cody et al., 2008, 2012; Crampton et al., 2016). This novel approach seeks to confront regional disparity in the timing of established biostratigraphic events and represents a significant step forward in understanding the timing and pacing of Cenozoic climate events. However, given that this CONOP-based biostratigraphy was developed from previously existing records with existing issues around sedimentation rate, poor-quality magnetostratigraphy and gaps in core recovery mentioned above apply to the ages used in the novel statistical assessment. A more recent CONOP-based study (Crampton et al., 2016) assessed the relationship between orbital parameters, ice, and diatom biogeography and found that five major episodes of cooling over the past 15 million years have led to significant species turnover (Crampton et al., 2016). Table 2 compares the dates of Cody et al. (2008) and Crampton et al. (2016) to those found here.

Overwhelmingly, the dates found here are within the dates provided by the average range model of Cody et al. (2008) or fall within 100–200 kyr. Notable exceptions are the first occurrences of several species which Cody et al. (2008) and authors of the works used therein place millions of years before we do. This is mostly likely due to ecological or taphonomic factors at Site U1537; these species were not found in this habitat or were not preserved in the sediments here during the early parts of their temporal range. Due to the high sedimentation rate of Site U1537, the close match to the EPICA Dome C ice core dust record allowing precise orbital tuning (Weber et al., 2022), and the detailed paleomagnetic record in the lower portions of the core (Reilly et al., 2021), the dates provided here are ideal for biostratigraphic work, excepting the anomalous FO dates (specifically those of *A. ingens*, *H. karstenii*, *Th. torokina*, *P. barboi*, and *Th. oliverana*). Comparison to Crampton et al. (2016) is more enigmatic. Many dates are somewhat similar, falling within 200–300 kyr, e.g., the LO of *Th. vulnifica*, which is reported at 2.06 Ma by Crampton et al. (2016) and at 2.098 Ma here. In other cases, the differences are extreme, e.g., the FO of *F. separanda*, which was reported at 0.47 Ma by Crampton et al. (2016) and at 1.242 Ma here. While fossil reworking can lead to a false LO, these processes cannot alter an FO date. Therefore, we recommend using the scheme presented here for FO data presented in Crampton et al. (2016). Similarly to Cody et al. (2008), the oldest dates in Crampton et al. (2016) are recommended over those provided here due to sampling (e.g., FO datums for *A. ingens*, *H. karstenii*, *Th. torokina*, *P. barboi*, and *Th. oliverana*).

Data availability. Data sets used in this paper are available upon request.

Supplement. The supplement related to this article is available online at https://doi.org/10.5194/jm-44-497-2025-supplement.

Author contributions. Initial shipboard diatom analyses were performed by JW, LA, and YK. Subsequent diatom analyses were performed by JW. BR applied the age model and generated figures. JW generated figures and tables.

Competing interests. The contact author has declared that none of the authors has any competing interests.

Disclaimer. Publisher's note: Copernicus Publications remains neutral with regard to jurisdictional claims made in the text, published maps, institutional affiliations, or any other geographical representation in this paper. While Copernicus Publications makes every effort to include appropriate place names, the final responsibility lies with the authors.

Acknowledgements. This research used samples provided by the International Ocean Discovery Program (IODP). We would like to thank the dedicated crew of the D/V *JOIDES Resolution* and the expedition scientists. We thank the reviewers for helping to develop this article and improve it. Funding for this research was provided by an IODP Post-Expedition Award to Jonathan P. Warnock.

Financial support. This research has been supported by the US Science Support Program, Lamont-Doherty Earth Observatory (grant no. PEA).

Review statement. This paper was edited by Christina Riesselman and reviewed by Grace Duke and one anonymous referee.

References

Amante, C. and Eakins, B. W.: ETOPO1 1 arc-minute global relief model: procedures, data sources and analysis, NOAA Technical Memorandum, NESDIS, NGDC-24, 2009.

Arndt, J. E. Schenke, H. W. Jakobsson, M., Nitsche, F. O., Buys, G., Goleby, B., Rebesco, M., Bohoyo, F., Hong, J. Black, J., Greku, R., Udintsev, G., Barios, F., Reynoso-Peralta, W., Taisie, M., and Wigley, R.: The International Bathymetric Chart of the Southern Ocean (IBSCO) Version 1.0 – A new bathymetric compilation covering circum-Antarctic waters, Geophys. Res. Lett., 40, 3111–3117, https://doi.org/10.1002/grl.50413, 2013.

Arney, J. E., McGonigal, K. L., Ladner, B. C., and Wise Jr., S. W.: Lower Oligocene to middle Miocene diatom biostratigraphy of ODP Site 1140, Kerguelen Plateau, in: Proc. ODP, Sci. Results, 183, edited by: Frey, F. A., Coffin, M. F., Wallace, P. J., and Quilty, P. G., College Station, TX (Ocean Drilling Program), 1–21, https://doi.org/10.2973/odp.proc.sr.183.009.2003, 2003.

Anderson, J. B. and Andrews, J. T.: Radiocarbon constraints on ice sheet advance and retreat in the Weddell Sea, Antarctica, Geology, 27, 179–182, https://doi.org/10.1130/0091-7613(1999)027<0179:RCOISA>2.3.CO;2, 1999.

Bailey, I., Hemming, S., Reilly, B. T., Rollinson, G., Williams, T., Weber, M. E., Raymo, M. E., Peck, V. L., Ronge, T. A., Brachfeld, S., O'Connell, S., Tauxe, L., Warnock, J. P., Armbrecht, L., Cardillo, F. G., Du, Z., Fauth, G., Garcia, M., Glueder, A., Guitard, M., Gutjahr, M., Hernández-Almeida, I., Hoem, F. S., Hwang, J., Iizuka, M., Kato, Y., Kenlee, B., Martos, Y. M., Pérez, L. F., Seki, O., Tripathi, S., and Zheng, X.: Episodes of Early Pleistocene West Antarctic Ice Sheet Retreat Recorded by Iceberg Alley Sediments, Paleoceanogr. Paleocl., 37, e2022PA004433, https://doi.org/10.1029/2022PA004433, 2022.

Baldauf, J. G. and Barron, J. A.: Diatom biostratigraphy: Kerguelen Plateau and Prydz Bay regions of the Southern Ocean, in: Proc. ODP, Sci. Results, 119, edited by: Barron, J., Larsen, B., Baldauf, J. G., Alibert, C., Berkowitz, S., Caulet, J.-P., Chambers S., Cooper, A., Cranston, R., Dorn, W., Ehrmann, W., Fox, R., Fryxell, G., Hambrey, M., Huber, B., Jenkins, C., Kang, S.-H., Keating, B., Mehl, K., Noh, I., Ollier, G., Pittenger, A., Sakai, H., Schroder, C., Solheim, A., Stockwell, D., Thierstein, H., Tocher, B., Turner, B., and Wei, W., College Station, TX (Ocean Drilling Program), 547–598, https://doi.org/10.2973/odp.proc.sr.119.135.1991, 1991.

Barron, J. A.: Planktonic Marine Diatom Record Of The Past 18 M.Y.: Appearances and Extinctions in the Pacific and Southern Oceans, Diatom Res., 18, 203–224, https://doi.org/10.1080/0269249X.2003.9705588, 2003.

Bohaty, S. M., Wise Jr., S. W., Duncan, R. A., Moore, C. L., and Wallace, P. J.: Neogene diatom biostratigraphy, tephra stratigraphy, and chronology of ODP Hole 1138A, Kerguelen Plateau, in: Proc. ODP, Sci. Results, 183, edited by: Frey, F. A., Coffin, M. F., Wallace, P. J., and Quilty, P. G., College Station, TX (Ocean Drilling Program), 1–53, https://doi.org/10.2973/odp.proc.sr.183.016.2003, 2003.

Bohaty, S. M., Scherer, R. P., and Harwood, D. M.: Quaternary diatom biostratigraphy and palaeoenvironments of the CRP-1 drillcore, Ross Sea, Antarctica, Terra Ant., 5, 431–454, 1998.

Budge, J. S. and Long, D. G.: A Comprehensive Database for Antarctic Iceberg Tracking Using Scatterometer Data, IEEE J. Sel. Top. Appl., 11, 434–442, https://doi.org/10.1109/JSTARS.2017.2784186, 2018.

Censarek, B. and Gersonde, R.: Miocene diatom biostratigraphy at ODP Sites 689, 690, 1088, 1092 (Atlantic sector of the Southern Ocean), Mar. Micropaleontol., 45, 309–356, https://doi.org/10.1016/S0377-8398(02)00034-8, 2002.

Ciesielski, P. F.: The Neogene and Quaternary diatom biostratigraphy of subantarctic sediments, Deep Sea Drilling Project Leg 71, in: Init Rep DSDP, 71, edited by: Ludwig, W. J., Krasheninnikov, V. A., Basov, I. A., Bayer, U., Bloemendal, J., Bornhold, B., Ciesielski, P. F., Goldstein, E. H., Robert, C., Salloway, J., Usher, J. L., von der Dick, H., Weaver, F. M., and Wise Jr., S. W., Washington, DC (U.S. Government Printing Office), 635–666, https://doi.org/10.2973/dsdp.proc.71.125.1983, 1983.

Cody, R., Levy, R., Crampton, J., Naish, T., Wilson, G., and Harwood, D.: Selection and stability of quantitative stratigraphic age models: Plio-Pleistocene glaciomarine sediments in the ANDRILL 1B drillcore, McMurdo Ice Shelf, Global Planet. Change, 96–97, 143–156, https://doi.org/10.1016/j.gloplacha.2012.05.017, 2012.

Cody, R. D., Levy, R. H., Harwood, D. M., and Sadler, P. M.: Thinking outside the zone: High-resolution quantitative diatom biochronology for the Antarctic Neogene. Palaeogeogr. Palaeocl., 260, 92–121, https://doi.org/10.1016/j.palaeo.2007.08.020, 2008.

Crampton, J. S., Cody, R. D., Levy, R., Harwood, D., McKay, R., and Naish, T. R.: Southern Ocean phytoplankton turnover in response to stepwise Antarctic cooling over the past 15 million years, P. Natl. Acad. Sci. USA, 113, 6868–6873, https://doi.org/10.1073/pnas.1600318113, 2016.

Fenner, J.: Late Pliocene–Quaternary diatom stratigraphy in the Atlantic sector of the Southern Ocean, in: Proc. ODP, Sci. Results, 114, edited by: Ciesielski, P. F., Kristoffersen, Y., Clement, B., Blangy, J.-P., Borrouilh, R., Crux, J. Z., Fenner, J. M., Froelich, P. N., Hailwood, E., Hodell, D., Katz, M. E., Ling, H. Y., Mienert, J., Müller, D., Mwenifumbo, C. J., Nobes, D. C., Nocchi, M., Warnke, D. A., and Westall, F., College Station, TX (Ocean Drilling Program), 97–121, https://doi.org/10.2973/odp.proc.sr.114.187.1991, 1991.

Gersonde, R.: Taxonomy and morphostructure of late Neogene diatoms from the Maude Rise (Antarctic Ocean), Polarforschung, 59, 141–171, 1991.

Gersonde, R. and Bárcena, M. A.: Revision of the Upper Pliocene: Pleistocene Diatom Biostratigraphy for the Northern Belt of the Southern Ocean, Micropaleontology, 44, 84–98, https://doi.org/10.2307/1486086, 1998.

Gersonde, R. E. and Burckle, L. H.: Neogene diatom biostratigraphy of ODP Leg 113, Weddell Sea (Antarctic Ocean), Proceedings of the Ocean Drilling Program, Scientific Results, Proceedings of the Ocean Drilling Program, Weddell Sea, Antarc-

tica, covering Leg 113 of the cruises of the Drilling Vessel JOIDES Resolution, Valparaiso, Chile, to East Cove, Falkland Islands, sites 689–697, 25 December 1986–11 March 1987, College Station, TX (Ocean Drilling Program), 113, 761–789, https://doi.org/10.2973/odp.proc.sr.113.126.1990, 1990.

Gombos Jr., A. M.: Paleogene and Neogene diatoms from the Falkland Plateau and Malvinas Outer Basin: Leg 36, Deep Sea Drilling Project, in: Initial Reports of the Deep Sea Drilling Project, 36, edited by: Barker, P. F. and Dalziel, I. W. D., Washington, DC (U.S. Government Printing Office), 575–687, https://doi.org/10.2973/dsdp.proc.36.111.1977, 1976.

Gombos Jr., A. M.: A new diatom genus from the early Paleocene, Bacillaria, 6, 237–244, 1983.

Gradstein, F., Ogg, J., Schmitz, M., and Ogg, G. (Eds.): Geologic Time Scale, Elsevier, https://doi.org/10.1016/C2020-1-02369-3, 2020.

Harwood, D. M.: Diatoms, in: Antarctic Cenozoic History from the MSSTS-1 Drillhole, edited by: Barrett, P. J., McMurdo Sound, DSIR Bulletin (New Zealand), 237, 69–107, 1986.

Harwood, D. M.: Siliceous microfossils, in: Antarctic Cenozoic History from the CIROS-1 Drillhole, edited by: Barrett, P. J., McMurdo Sound, DSIR Bulletin (New Zealand), 245, 67–97, 1989.

Harwood, D. M. and Bohaty, S. M.: Early Oligocene siliceous microfossil biostratigraphy of Cape Roberts Project core CRP-3, Victoria Land Basin, Antarctica, Terra Ant., 8, 315–338, 2001.

Harwood, D. M. and Maruyama, T.: Middle Eocene to Pleistocene diatom biostratigraphy of Southern Ocean sediments from the Kerguelen Plateau, LEG 120, edited by: Wise, Jr., S. W., Palmer Julson, A. A., Schilich, R., and Thomas, E., Proc. ODP, Sci. Results, 120, 683–733, https://doi.org/10.2973/odp.proc.sr.120.160.1992, 1992.

Harwood, D. M., Bohaty, S. M., and Scherer, R. P.: Lower Miocene diatom biostratigraphy of the CRP-1 drillcore, McMurdo Sound, Antarctica, Terra Ant., 5, 499–514, 1998.

Iwai, M. and Winter, D.: Data report: taxonomic notes of Neogene diatoms from the western Antarctic peninsula, Ocean Drilling Program Leg 178, in: Proc. ODP, Sci. Results 178, edited by: Barker, P. F., Camerlenghi, A., Acton, G. D., and Ramsay, A. T. S., College Station, TX (Ocean Drilling Program), 1–57, https://doi.org/10.2973/odp.proc.sr.178.239.2002, 2002.

Kato, Y., Hernández-Almeida, I., and Pérez, L. F.: Diatom and radiolarian biostratigraphy in the Pliocene sequence of ODP Site 697 (Jane Basin, Atlantic sector of the Southern Ocean), J. Micropalaeontol., 43, 93–119, https://doi.org/10.5194/jm-43-93-2024, 2024.

Kato, Y., Onodera, J., Suto, I., Teraishi, A., and Takahashi, K.: Pliocene and Pleistocene paleoceanography in the western subarctic Pacific based on diatom analyses of ODP Leg 145 Hole 884B and IODP Expedition 323 Holes U1341B and U1343E, Deep-Sea Res. Pt. II, 125–126, 29–37, https://doi.org/10.1016/j.dsr2.2015.04.004, 2016.

Kellogg, D. E. and Kellogg, T. B.: Diatom Biostratigraphy of Sediment Cores from beneath the Ross Ice Shelf, Micropaleontology, 32, 74–94, https://doi.org/10.2307/1485703, 1986.

Konfirst, M. A., Scherer, R. P., Hillenbrand, C.-D., and Kuhn, G.: A marine diatom record from the Amundsen Sea – Insights into oceanographic and climatic response to the Mid-Pleistocene Transition in the West Antarctic sector of the Southern Ocean, Mar. Micropaleontol., 92–93, 40–51, https://doi.org/10.1016/j.marmicro.2012.05.001, 2012.

Lambert, F., Delmonte, B., Petit, J. R., Bigler, M., Kaufmann, P.R., Hutterli, M. A., Stocker, T. F., Ruth, U., Steffensen, J. P., and Maggi, V.: Dust-climate couplings over the past 800,000 years from the EPICA Dome C ice core, Nature, 452, 616–619, https://doi.org/10.1038/nature06763, 2008.

Lisiecki, L. E. and Raymo, M. E.: A Pliocene-Pleistocene stack of 57 globally distributed benthic δ^{18}O records, Paleoceanography, 20, 2004PA001071, https://doi.org/10.1029/2004PA001071, 2005.

Liu, H., Li, X.-M., and Guo, H.: The Dynamic Processes of Sea Ice on the East Coast of Antarctica – A case study based on Spaceborne Synthetic Aperture Radar Data from TerraSAR-X, IEEE J. Sel. Top. Appl., 9, 1187–1198, https://doi.org/10.1109/JSTARS.2015.2497355, 2016.

Lougheed, B. C. and Obrochta, S. P.: A Rapid, Deterministic Age-Depth Modeling Routine for Geological Sequences With Inherent Depth Uncertainty, Paleoceanogr. Paleocl., 34, 122–133, https://doi.org/10.1029/2018PA003457, 2019.

Mahood, A. D. and Barron, J. A.: Late Pliocene Diatoms in a Diatomite from Prydz Bay, East Antarctica, Micropaleontology, 42, 285–302, https://doi.org/10.2307/1485876, 1996.

Matsuoka, K., Skoglund, A., Roth, G., de Pomereu, J., Griffiths, H., Headland, R., Herried, B., Katsumamta, K., Le Brocq, A., Licht, K., Morgan, F., Neff, P.D., Ritz, C., Scheinert, M., Tamura, T., Van de Putte, A., ban den Broeke, M., von Deschwanden, A., Deschamps-Berger, C., Van Liefferinge, B., and Melvær, Y.: Quantarctica, an integrated mapping environment for Antarctica, the Southern Ocean, and sub-Antarctic islands, Environ. Model. Softw., 140, 105015, https://doi.org/10.1016/j.envsoft.2021.105015, 2021.

McCollum, D. W.: Diatom Stratigraphy of the Southern Ocean Initial Report Deep Sea, 28, Washington, DC (U.S. Government Printing Office), edited by: Kaneps, A. G., https://doi.org/10.2973/dsdp.proc.28.112.1975, 1975.

Olney, M. P., Scherer, R. P., Harwood, D. M., and Bohaty, S. M.: Oligocene–early Miocene Antarctic nearshore diatom biostratigraphy, Deep-Sea Res., 54, 2325–2349, https://doi.org/10.1016/j.dsr2.2007.07.020, 2007.

Olney, M. P., Bohaty, S. M., Harwood, D. M., and Scherer, R. P.: *Crenia lacyae* gen. nov. et sp. nov. and *Synedropsis cheethamii* sp. nov., Fossil indicators of Antarctic sea ice?, Diatom. Res., 24, 357–375, https://doi.org/10.1080/0269249X.2009.9705807, 2009.

Orsi, A. H., Whitworth III, T., and Nowlin, Jr., W. D.: On the meridional extent and fronts of the Antarctic Circumpolar Current, Deep-Sea Res. Pt. I, 42, 641–673, https://doi.org/10.1016/0967-0637(95)00021-W, 1995.

Pérez, L. F., Martos, Y. M., García, M., Weber, M. E., Raymo, M. E., Williams, T., Bohoyo, F., Armbrecht, L., Bailey, I., Brachfeld, S., Glüder, A., Guitard, M., Gutjahr, M., Hemming, S., Hernández-Almeida, I., Hoem, F. S., Kato, Y., O'Connell, S., Peck, V. L., Reilly, B., Ronge, T. A., Tauxe, L., Warnock, J., and Zheng, X.: Miocene to present oceanographic variability in the Scotia Sea and Antarctic ice sheets dynamics: Insight from revised seismic-stratigraphy following IODP Expedition 382, Earth Planet. Sc. Lett., 553, 116657, https://doi.org/10.1016/j.epsl.2020.116657, 2021.

Reilly, B. T., Tauxe, L., Brachfeld, S., Raymo, M., Bailey, I., Hemming, S., Weber, M. E., Williams, T., Garcia, M., Guitard, M., Martos, Y. M., Pérez, L. F., Zheng, X., Armbrecht, L., Cardillo, F. G., Du, Z., Fauth, G., Glueder, A., Gutjahr, M., Hernández-Almeida, I., Hoem, F. S., Hwang, J., Iizuka, M., Kato, Y., Kenlee, B., O'Connell, S., Peck, V., Ronge, T. A., Seki, O., Tripathi, S., and Warnock, J.: New Magnetostratigraphic Insights From Iceberg Alley on the Rhythms of Antarctic Climate During the Plio-Pleistocene, Paleoceanogr. Paleocl., 36, e2020PA003994, https://doi.org/10.1029/2020PA003994, 2021.

Scherer, R., Bohaty, S. M., and Harwood, D. M.: Oligocene and lower Miocene siliceous microfossil biostratigraphy of Cape Roberts project core CRP-2/2A, Victoria land basin, Antarctica, Terra Ant., 7, 417–442, 2000.

Schrader, H.-J.: Cenozoic planktonic diatom biostratigraphy of the Southern Pacific Ocean, edited by: Hollister, C. D., Craddock, C., Bogdanov, Y. A., Edgar, N. T., Gieskes, J. M., Haq, B. U., Lawrence, J. R., Rögl, R., Schrader, H.-J., Tucholke, B. E., Bennum, W. R., Weaver, F. M., and Zhivago, V. N., Init. Rep. Deep Sea, 35, Washington, DC (U.S. Government Printing Office), 605–671, https://doi.org/10.2973/dsdp.proc.35.136.1976, 1976.

Sjunneskog, C. and Scherer, R. P.: Mixed diatom assemblages in glacigenic sediment from the central Ross Sea, Antarctica, Palaeogeogr. Palaeocl., 218, 287–300, https://doi.org/10.1016/j.palaeo.2004.12.019, 2005.

Sjunneskog, C. and Winter, D.: A diatom record of late Pliocene cooling from the Ross Sea continental shelf, AND-1B Antarctica, Global Planet. Change, 96–97, 87–96, https://doi.org/10.1016/j.gloplacha.2012.01.013, 2012.

Sjunneskog, C., Riesselman, C., Winter, D., and Scherer, R.: *Fragilariopsis* diatom evolution in Pliocene and Pleistocene Antarctic shelf sediments, Micropaleontology, 58, 273–289, 2012.

Spreen, G., Kaleschke, L., and Heygster, G.: Sea ice remote sensing using ASMR-E 89-GHz channels, J. Geophys. Res.-Oceans, 113, C02S03, https://doi.org/10.1029/2005JC003384, 2005.

Sprenk, D., Weber, M. E., Kuhn, G., Rośen, P., Frank, M., Molina-Kescher, M., Liebetrau, V., and Röhling, H.-G.: Southern Ocean bioproductivity during the last glacial cycle – new detection method and decadal-scale insight from the Scotia Sea, Geol. Soc. Lond. Spec. Publ., 381, 245–261, 2013.

Tauxe, L., Stickley, C. E., Sugisaki, S., Bijl, P. K., Bohaty, S. M., Brinkhuis, H., Escutia, C., Flores, J. A., Houben, A. J. P., Iwai, M., Jiménez-Espejo, F., McKay, R., Passchier, S., Pross, J., Riesselman, C. R., Röhl, U., Sangiorgi, F., Welsh, K., Klaus, A., Fehr, A., Bendle, J. A. P., Dunbar, R., Gonzàlez, J., Hayden, T., Katsuki, K., Olney, M. P., Pekar, S. F., Shrivastava, P. K., Van De Flierdt, T., Williams, T., and Yamane, M.: Chronostratigraphic framework for the IODP Expedition 318 cores from the Wilkes Land Margin: Constraints for paleoceanographic reconstruction, Paleoceanography, 27, 2012PA002308, https://doi.org/10.1029/2012PA002308, 2012.

Tolotti, R., Bárcena, M. A., Macrì, P., Caburlotto, A., Bonci, M. C., De Santis, L., Donda, F., Corradi, N., and Crosta, X.: Wilkes Land Late Pleistocene diatom age model: From bio-events to quantitative biostratigraphy, Revue de Micropaléontologie, 61, 81–96, https://doi.org/10.1016/j.revmic.2018.05.001, 2018.

Warnock, J. P. and Scherer, R. P.: Diatom species abundance and morphologically-based dissolution proxies in coastal Southern Ocean assemblages, Cont. Shelf Res., 102, 1–8, https://doi.org/10.1016/j.csr.2015.04.012, 2015.

Warnock, J. P., Reilly, B. T., Raymo, M. E., Weber, M. E., Peck, V., Williams, T., Armbrecht, L., Bailey, I., Brachfeld, S., Du, Z., Fauth, G., García, M. M., Glüder, A., Guitard, M., Gutjahr, M., Hemming, S., Hernández-Almeida, I., Hoem, F. S., Hwang, J., Iizuka, M., Kato, Y., Lee, B., Martos, Y. M., O'Connell, S., Pérez, L. F., Ronge, T. A., Seki, O., Tauxe, L., Tripathi, S., Zheng, X., Stoner, J., and Scherer, R. P.: Latitudinal Variance in the Drivers and Pacing of Warmth During Mid-Pleistocene MIS 31 in the Antarctic Zone of the Southern Ocean, Paleoceanogr. Paleocl., 37, e2021PA004394, https://doi.org/10.1029/2021PA004394, 2022.

Weaver, F. M. and Gombos Jr., A. M.: Southern High-Latitude diatom biostratigraphy, SEPM Spec. Pub., 32, 445–470, 1981.

Weber, M. E., Raymo, M. E., Peck, V. L., and Williams, T. (Eds.): Volume 382: Iceberg Alley and Subantarctic Ice and Ocean Dynamics, Proc. Int. Ocean Dis. Prog. International Ocean Discovery Program, Texas A&M University, https://doi.org/10.14379/iodp.proc.382.2021, 2021.

Weber, M. E., Bailey, I., Hemming, S. R., Martos, Y. M., Reilly, B. T., Ronge, T. A., Brachfeld, S., Williams, T., Raymo, M., Belt, S. T., Smik, L., Vogel, H., Peck, V. L., Armbrecht, L., Cage, A., Cardillo, F. G., Du, Z., Fauth, G., Fogwill, C. J., Garcia, M., Garnsworthy, M., Glüder, A., Guitard, M., Gutjahr, M., Hernández-Almeida, I., Hoem, F. S., Hwang, J.-H., Iizuka, M., Kato, Y., Kenlee, B., OConnell, S., Pérez, L. F., Seki, O., Stevens, L., Tauxe, L., Tripathi, S., Warnock, J., and Zheng, X.: Antiphased dust deposition and productivity in the Antarctic Zone over 1.5 million years, Nat. Commun., 13, 2044, https://doi.org/10.1038/s41467-022-29642-5, 2022.

Whitehead, J. M. and Bohaty, S. M.: Data report: Quaternary–Pliocene diatom biostratigraphy of ODP Sites 1165 and 1166, Cooperation Sea and Prydz Bay, in: Proc. ODP, Sci. Results, 188, edited by: Cooper, A. K., O'Brien, P. E., and Richter, C., College Station, TX (Ocean Drilling Program), 1–25, https://doi.org/10.2973/odp.proc.sr.188.008.2003, 2003.

Winter, D., Sjunneskog, C., Scherer, R., Maffioli, P., Riesselman, and C., Harwood, D.: Pliocene–Pleistocene diatom biostratigraphy of nearshore Antarctica from the AND-1B drillcore, McMurdo Sound, Global Planet. Change, 96–97, 59–74, https://doi.org/10.1016/j.gloplacha.2010.04.004, 2012.

Winter, D. M. and Harwood, D. M.: Integrated diatom biostratigraphy of late Neogene drillholes in Southern Victoria Land and correlation to Southern Ocean records, in: The Antarctic Region: Geological Evolution and Processes, edited by: Ricci, C. A., Terra Ant. Pub., 985–992, 1997.

Winter, D. M. and Iwai, M.: Neogene diatom biostratigraphy, Antarctic Peninsula Pacific margin, ODP Leg 178 rise sites, Proc. ODP, Sci. Results, 178, 25, https://doi.org/10.2973/odp.proc.sr.178.230.2002, 2002.

Zielinski, U. and Gersonde, R.: Plio–Pleistocene diatom biostratigraphy from ODP Leg 177, Atlantic sector of the Southern Ocean, Mar. Micropaleontol., 45, 225–268, https://doi.org/10.1016/S0377-8398(02)00031-2, 2002.